PERGAMON

Journal of Structural Geology 21 (1999) 419–436

JOURNAL OF STRUCTURAL GEOLOGY

Shape preferred orientations of survivor grains in fault gouge

Trenton T. Cladouhos *

Department of Geological Sciences, Box 351310, University of Washington, Seattle, WA 98195, USA

Received 1 November 1996; accepted 11 December 1998

Abstract

Survivor grains are rounded, isolated clasts in fault gouge that escaped the grain fracturing so evident in fault breccia. Surrounded by a matrix of clay or comminuted parent rock, they are free to rotate without interference from other clasts. Using an optical microscope, electron microprobe images, and image analysis software, I collected data on the long axis orientations of elongate ($a/b > 1.4$) survivors in 15 samples of fault gouge and breccia from Death Valley, California. Survivor grains display a profound shape preferred orientation (SPO) which can be used to infer kinematic parameters of gouge deformation. The SPO depends on the gouge type. In clay gouge the SPO is inclined to the shear plane, similar to the P-foliation usually defined by a phyllosilicate fabric. In flow-banded granular gouge the SPO is parallel to the shear plane and banding. To explore the implications of the SPO data, kinematic models of passive markers in simple shear (March model), rigid ellipsoids in simple shear (Jeffery model), and rigid ellipsoids in general shear (Ghosh and Ramberg model) were numerically implemented. Comparison of SPO data and model results suggests two explanations for the inclined SPO of clay gouge: either the simple shear strain experienced by clay gouge is low ($\gamma<4$) or the shear strain is unlimited but gouge deformation included apparent thickening of the shear zone. In the accompanying paper the latter option is assumed and a kinematic model of brittle shear zones which includes another commonly observed microstructure of fault gouge, Riedel shears, is developed to explain the inclined SPO in clay gouge.

1. Introduction

Description and analysis of microstructures within fault gouge and breccia—the products of faulting at low ($<250^{\circ}C$) temperatures and shallow depths—are rare. It is unknown whether the few field studies of gouge from strike-slip (Rutter et al., 1986; Chester and Logan, 1987) and thrust (Erickson, 1990; Erickson and Wiltschko, 1991) faults are generally applicable. Despite the paucity of descriptions of natural gouge and breccia with which to compare experimental results, several recent efforts to understand the mechanics of gouge-filled faults in the laboratory have been proposed (Scott et al., 1994; Beeler and Tullis, 1995; Blanpied et al., 1995). In this paper I describe an important microstructural feature of natural fault gouge from a low angle normal fault—shape preferred orientation of survivor grains—that may provide important clues to the characteristics of deformation within gouge.

The turtleback faults on the east flank of southern Death Valley are superbly exposed, offering an unprecedented natural laboratory for studying the microstructures and kinematics of fault rocks (Fig. 1). The extremely dry climate ensures that the fault gouge and breccia, ordinarily water-saturated and incohesive, are dry, cohesive, and relatively easy to sample. About one meter of breccia and gouge are typically exposed along the low-angle detachment faults of Death Valley. I interpret that most of the shear was concentrated in the finest-grained material, a 10–30 cm zone of flow-banded or foliated gouge adjacent to the hanging wall. Within this unit a pronounced shape preferred orientation (SPO, Shelley, 1993, p. 317) is revealed by careful measurement of the orientations of long axes of elliptical particles. In most gouge the SPO is not

* Also at: Golder Associates Inc., 4104 148th Avenue NE, Redmond, WA 98052, USA.

E-mail address: tcladouhos@golder.com (T. Cladouhos)

0191-8141/99 $ - see front matter
PII: S0191-8141(98)00123-0

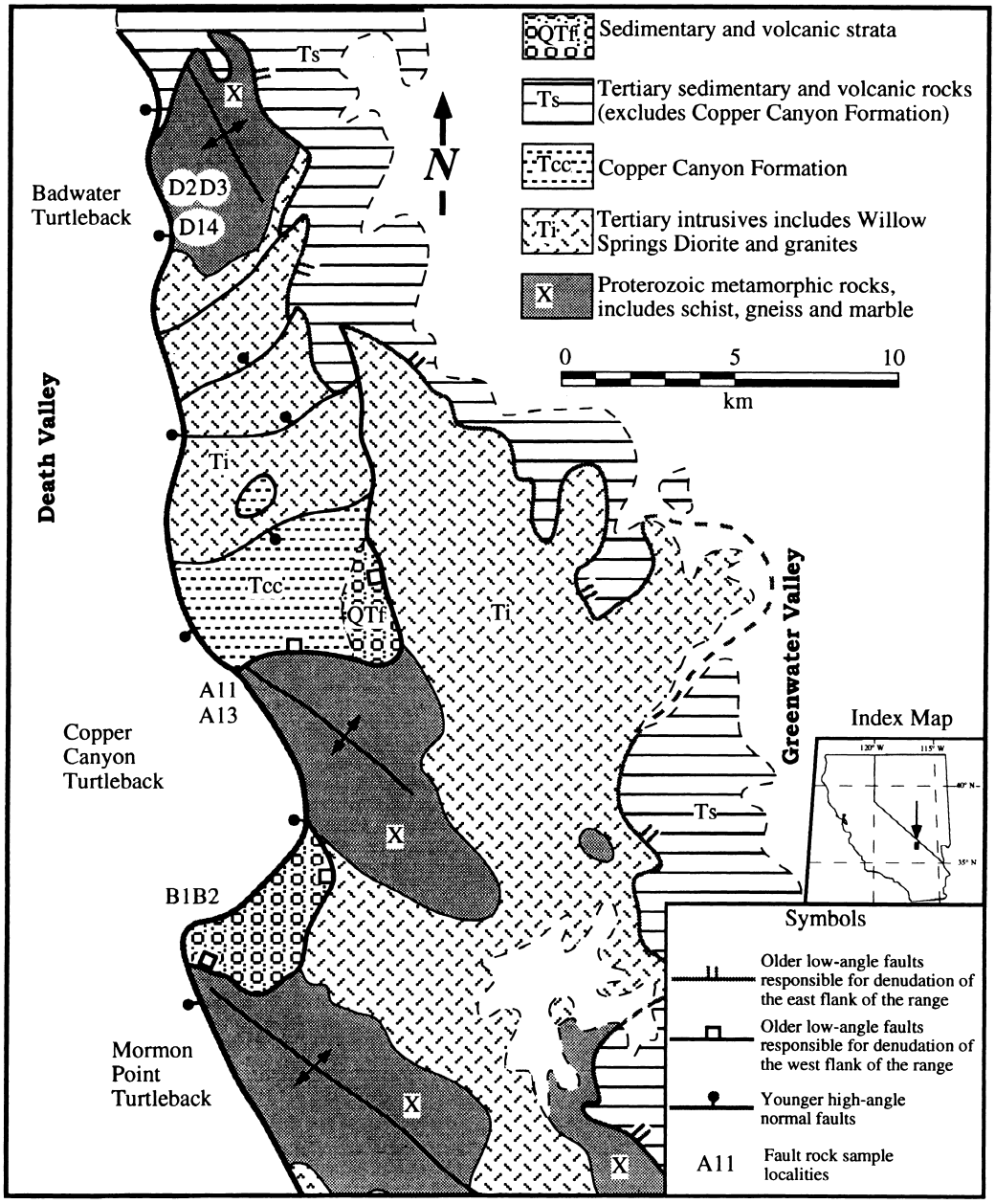

Fig. 1. Simplified geologic map of the Black Mountains, Death Valley National Park, California. Redrafted from Drewes (1963) and Holm and Wernicke (1990).

apparent to the eye in either outcrop or thin section. Because the particles are free to rotate within a matrix of clay and other fine-grained material without interference from similar sized grains, I believe that the SPO of survivor grains can be used to determine the ratio of pure shear rate to simple shear rate in a granular flow. To test this hypothesis, the results of numerical modeling are compared to the data collected from natural rocks. In an accompanying paper (Cladouhos, 1999), a kinematic model is developed that incorporates Riedel shears and granular flow to explain the orientations of the SPO.

2. Fault rock terminology

Faults in the upper 10–15 km of the earth's crust are generally marked by a zone of rocks which have been fractured into clasts during brittle deformation and are collectively called *cataclastic rocks*. Cohesive cataclastic rocks, thought to have formed deeper than

Table 1
Summary of observations made of thin sections used in SPO study

Sample	Locality	% Visible fragments*	Clast shapes	Local shear evidence†	Descriptive name
A1	Copper Canyon TB	25	Subrounded	R1, R2	Immature foliated **clay gouge**
A3	Copper Canyon TB	26	Ang. & Round	R1, R2, Y	**Breccia** of gneiss
A6	Copper Canyon TB	15	Rounded	None	Flow banded **granular gouge**
A11	Copper Canyon TB	9	Rounded	R1	Foliated **clay gouge**
A13	Copper Canyon TB	15	Rounded	R1, Y	**Clay gouge** w/ weak foliation
B1	Mormon Point TB	26	Rounded	None	Flow banded **granular gouge**
B2	Mormon Point TB	23	Angular	R1	**Breccia** of gneiss
D2	Badwater TB	15	Rounded	None	Flow banded **granular gouge**
D3	Badwater TB	25	Angular	R1	**Breccia** of dolomitic marble
D11	Badwater TB	18	Rounded	R1	**Clay gouge** w/ weak foliation
D14	Badwater TB	1	Rounded	None	**Clay gouge** w/ weak foliation
CtLs‡	Keystone Thrust, Nevada	~50	Subrounded	R1, R2	**Breccia** of limestone

*At low (7×) magnification in thin section. †R1 = synthetic Riedel shear, R2 = antithetic Riedel shears, Y = shears parallel to fault plane. ‡Sample of cataclastic limestone loaned to us by C. Sammis. TB = Turtle Backs.

~4 km, are called *cataclasites* (Sibson, 1977; Wise et al., 1984; Scholz, 1990; Twiss and Moores, 1992). Incohesive cataclastic rocks, thought to have formed shallower than ~4 km (i.e. fig. 4.4 of Twiss and Moores, 1992), are called *fault gouge* or *fault breccia* depending on the relative abundance of matrix and clasts. Although cohesiveness may not be the best fault rock discriminant because processes unrelated to the petrogenesis of fault rock may be responsible for the cohesiveness (i.e. post-kinematic cementation and water saturation), it seems a reasonable field criterion. Still, a fundamental point of confusion is the lack of a field test for distinguishing between cohesive and incohesive cataclastic rocks. For example, the cataclastic rocks of Death Valley featured in this study are cohesive enough in the field to sample with a hammer and chisel; thus they might be called cataclasites. However, these samples disaggregate quickly in water, so must be cemented with an epoxy in order to cut and thin sections. In most climates fault zones are saturated with water, in which case the Death Valley fault rocks would be incohesive; therefore, the terms fault gouge and fault breccia are applied to the rocks studied here.

A criterion for distinguishing between gouge and breccia is not explicit either. I make the distinction optically by examining samples in thin section at low magnification (~10×). Traditionally, *fault breccia* is composed of >30% visible fragments and *fault gouge* contains <30% visible fragments (Sibson, 1977). For the Death Valley fault rocks this measure is a poor divider because several samples have ~30% visible fragments (see Table 1). In this paper, classification is also based upon the angularity of the visible fragments; in fault breccia the visible fragments are angular and fractured and consist of >20% of the rock in thin section (Fig. 2a), while in fault gouge the fragments are rounded to subrounded and consist of <40% of the rock in thin section (Fig. 2c and e). Including fragment shape in the definitions of gouge and breccia suggests a predominant deformation mechanism for each incohesive cataclastic rock. The presence of fractured, angular grains indicate that in breccias, cataclastic flow—'deformation that involves continuous brittle fracturing of grains in a rock, with attendant frictional sliding and possibly rolling of fractured particles past one another' (Twiss and Moores, 1992)—was operative until deformation ceased.

In contrast to fault breccias, clear evidence of cataclastic flow is not preserved in fault gouge. In gouge, I call the visible fragments *survivor grains* to indicate that they escaped the grain fracturing so evident in fault breccias (see also Engelder, 1974). The matrix in gouge is composed of clay minerals (i.e. smectite, chlorite, saponite) (Fig. 2f) and/or extremely fine-grained (<10 μm) remnants of the parent rock (feldspar, quartz, and calcite) (Fig. 2d). Survivor grains are typically rounded to subrounded and little evidence for fracturing is evident in thin section down to low (~400×) magnifications. Thus once a fault gouge is formed, particulate or granular flow—deformation that 'involves the rolling and sliding of rigid particles past one another' (Twiss and Moores, 1992)—may have been operative. This idea is consistent with the suggestion of An and Sammis (1994) that when the particles in a gouge matrix are less than ~1 μm in diameter, the 'grinding limit' has been reached, and grain fracturing ceases. Whether the grinding limit is reached or not, it appears that survivor grains, cushioned from one another by a fine-grained matrix, can be worn but not fractured by neighboring small grains.

3. SPO background

Shape preferred orientation (SPO) is the arrangement of the long axes of non-equant grains into a non-

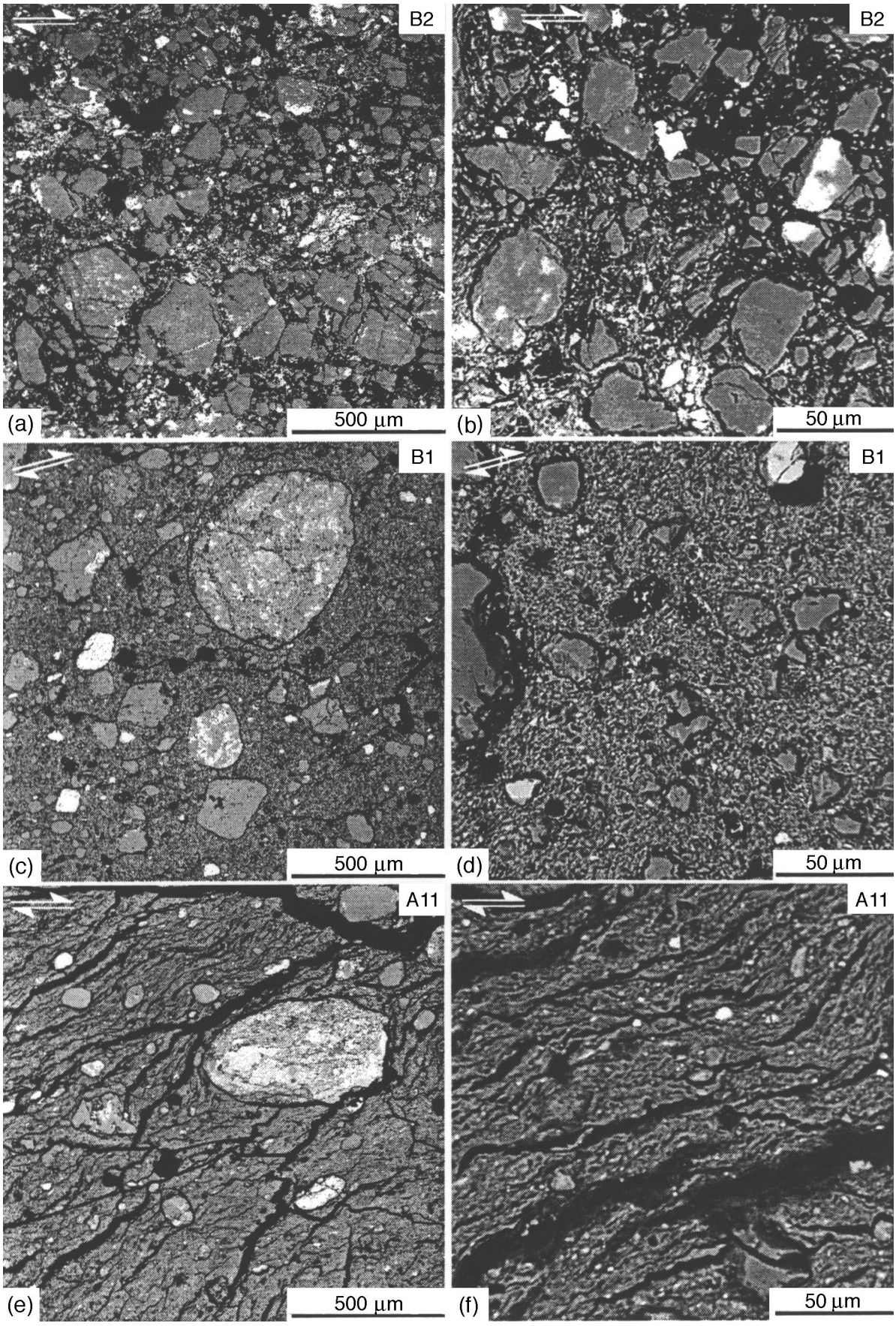

Fig. 2.

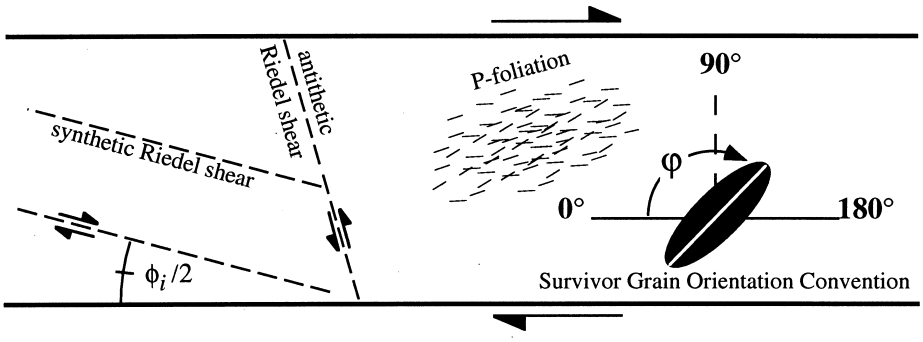

Fig. 3. Orientations of fabric elements in brittle shear zones and angle convention for the orientation of elliptical clasts.

random orientation (Shelley, 1993). Structural geologists have long recognized the record SPOs can provide for the strain history of deformed rocks (i.e. Sorby, 1853). Recent studies of SPO have focused primarily on mylonites, i.e. rocks deformed at crystal–plastic conditions (Hanmer and Passchier, 1991; Simpson and DePaor, 1993; Masuda et al., 1995; Shelley, 1995) because many geologists assume that brittle fault rocks are unfoliated (e.g. Wise et al., 1984). It has been recognized that some cataclasites can display a foliation defined by the preferred orientation of phyllosilicates and mineral segregations (Chester et al., 1985; Rutter et al., 1986; Chester and Logan, 1987; Blanpied et al., 1995); however no one has checked for SPO of grains in brittle fault rocks. Below I show that survivor grains *do* have a shape preferred orientation which also contributes to the fabric. Although these three independent fabric elements (shape preferred orientations, phyllosilicate preferred orientations, and mineral segregations) may not be exactly parallel, fabric elements inclined by 135–180° to the shear plane can collectively be called P-foliation (Logan et al., 1979; Rutter et al., 1986).

The recent work on the behavior of clasts in a deforming material is mostly theoretical (Simpson and DePaor, 1993), numerical (Masuda et al., 1995), or experimental (Passchier and Sokoutis, 1993). Two theoretical models of clast behavior in a shear zone are relevant to understanding SPO development. The quantitative details of the models are covered later; a brief introduction is appropriate now.

The simplest model was originally proposed by March (1932) and later refined by Oertel (1985). In this model, deformation within a shear zone is assumed to be simple shear and all material (clasts and matrix) within the zone is considered to be kinematically homogeneous. The rotation rate of any passive line depends only upon its orientation. The SPO of a set of initially randomly oriented lines will form near 135° and rotate with increased strain to a limit of 180° (see Fig. 3 for angle convention and sketch of fabric elements in brittle shear zones). The March model is generally accepted to be appropriate for predicting foliations across ductile (crystal–plastic) shear zones (i.e. Ramsay and Huber, 1983, pp. 33–54, 191–192). Chester and Logan (1987) extended the model to explain P-foliation orientations in brittle fault rocks from an extinct strand of the San Andreas fault. However, the March model treats objects as passive markers, thus may not be appropriate for modeling the rotation of rigid objects such as survivor grains. Two predictions of the March model are suspect: rigid clasts can only rotate 180° or less, and the long axes of elongate objects would become sensibly parallel to the shear plane at relatively low shear strains ($\gamma<10$).

An alternative approach to modeling the behavior of clasts was proposed by Jeffery (1922). In this model, clasts are treated as rigid ellipsoids embedded in a viscous matrix. Although the equations are general, the solutions presented by Jeffery (1922) are limited to 'laminar flow' or simple shear of the viscous matrix. The rotation rate of a rigid clast depends upon its orientation *and* shape (axial ratio). Unlike the March model, the Jeffery model predicts that individual clasts can rotate indefinitely.

The work of Ghosh and Ramberg (1976) unified the above two models as well as expanding both to include the possibility that deformation of the matrix could be characterized by general shear—a combination of pure shear and simple shear. The Ghosh and Ramberg (1976) model predicts that the rotation rate of a clast depends upon *s*, the ratio between simple shear rate

Fig. 2. Microprobe images of fault breccia and fault gouge from Death Valley samples. Sample B2 is a foliated breccia; Sample B1 a flow-banded granular gouge; and Sample A11 a foliated clay gouge. The flow-banding of Sample B1 is apparent in hand sample and optical thin section but not on this image. The images were created on a JEOL 800 microprobe in backscatter mode and then captured using Gatan's Digital Micrograph. The left column was collected at a probe magnification of 48× and the right column at 400×. The sense and orientation of shear is shown in the top left hand corner of each image and a scale bar in the bottom right corner.

and pure shear rate, and R, the axial ratio of the clast. In the Ghosh and Ramberg (1976) framework, the March model is simulated by setting $s = 0$ and $R = \infty$ and the Jeffery model is simulated by setting $s = 0$. Several workers have further developed the implications of the equations developed by Ghosh and Ramberg (1976) (Passchier and Simpson, 1986; Simpson and DePaor, 1993; Fossen et al., 1994; Masuda et al., 1995), but the field application of the model has been rather limited, even for rocks deformed at crystal–plastic conditions. Due to the model's inclusive nature and familiarity to many structural geologists, the SPO data will be compared to numerical results derived by using the Ghosh and Ramberg (1976) model. As with adopting any theoretical model, there are several uncertainties about the appropriateness of applying the Ghosh and Ramberg (1976) model to the shape preferred orientation of brittle fault rocks. Some of those uncertainties are explored in the discussion below.

4. The field study

4.1. Regional setting

The detachment fault system at the eastern edge of southern Death Valley (west flank of the Black Mountains) is composed of gently to moderately dipping (20–30°) extensional faults. Individual faults include the Badwater, Copper Canyon, and Mormon Point detachments, all of which are Miocene and younger in age (Holm and Wernicke, 1990). The total magnitude of normal slip on the fault system is debated; values range from over 50 km (Wernicke et al., 1988) to under 5 km (Wright and Troxel, 1984; Miller, 1992). Resolution of that debate is not crucial to this study; slip experienced under low temperature cataclastic conditions responsible for the gouge is at least 2 km. The Badwater, Copper Canyon, and Mormon Point detachments (collectively known as the Turtlebacks) separate a hanging wall of non-metamorphosed Tertiary and Quaternary volcanic and non-marine sedimentary rocks from a footwall of marble and crystalline plutonic and Precambrian metamorphic rocks.

Well-known geometry and timing, excellent fault rock exposure, and lack of post-kinematic alteration make the Death Valley turtlebacks the ideal locale for studying fault rocks. Field, petrologic, and isotopic studies (e.g. Drewes, 1963; Wright and Troxel, 1984; Wernicke et al., 1986; Miller, 1991a,b, 1992; Holm et al., 1992; Pavlis et al., 1993) have established the overall setting, character, and slip histories of these faults. The Copper Canyon detachment fault is exposed along an up-dip trace of more than 3 km; the Badwater and Mormon Point detachments are each exposed along strike for more than 3 km. Furthermore, many of the exposures are three-dimensional because the faults crop out on the walls of small canyons dissecting the turtlebacks. Most important, the sharp, planar detachment faults themselves form the upper boundaries of perfectly exposed brittle shear zones.

4.2. Simplified cross-section across a brittle shear zone and fault rock types

A typical outcrop of the fault zone includes (from bottom to top) fractured mylonitic footwall of chloritic schist, gneiss, or dolomitic marble, a 0.02–2 m thick zone of brittle fault rocks, a sharp detachment, and then undeformed clastic continental deposits (Fig. 4). At some exceptional exposures, fault gouge and fault breccias are up to 30 m thick.

A notable aspect of the zone of fault rocks is the wide variety of types present within the relatively narrow (0.02–2 m) zone. For descriptive purposes in

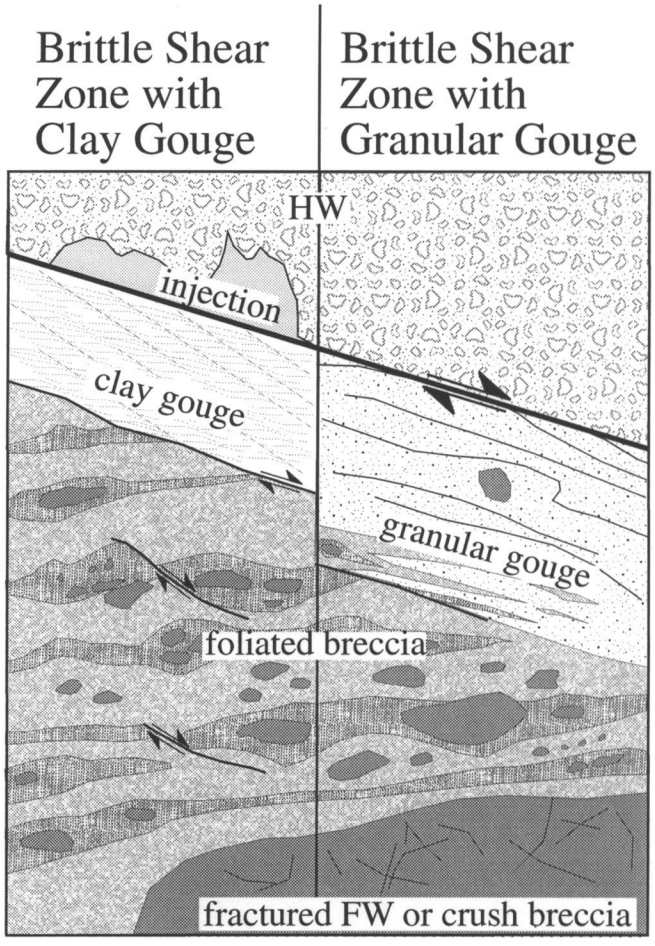

Fig. 4. Schematic cross-section of brittle shear zones observed in Death Valley.

the field, the fault rocks have been subdivided into three types: from the footwall up the types are foliated breccia, granular gouge, and clay gouge. Foliated breccia displays a coarse foliation defined by crushed lenses of footwall rock. Riedel shears are commonly visible in outcrop and thin section, giving this fault rock a composite P & R fabric (Cowan and Brandon, 1994). Granular gouge is characterized by a fault-plane-parallel flow-banding defined by mineral segregations, foliation, or boundinaged clasts and layers. Riedel shears are not visible in granular gouge. The matrix is green–orange and is composed of clay-sized grains, but not necessarily clay-minerals. We have not seen a description of this type of fault rock in the literature. Clay gouge is clay-rich, brick-red–brown, foliated, and contains dispersed millimeter-sized clasts. In thin sections, Riedel shears are visible in some clay gouges. This gouge type appears to be very mobile and can intrude or inject into the hanging wall, a phenomenon also described by Gretener (1977) along Cordilleran thrust faults and Engelder (1974) along some normal faults in the Southwestern U.S.

Although all three types of fault gouge are not always present, generally the types are asymmetrically zoned from the footwall to the detachment. Moving upward from the footwall, one first encounters in-place fractured footwall and/or crush breccias with little matrix and little evidence of shear. A fault breccia with footwall affinity of schist, gneiss, or marble follows. These breccias become finer grained, more matrix-rich and eventually a crude P & R composite fabric develops as the rock becomes a foliated breccia. Riedel shears are observed at both the microscale in foliated breccia and clay gouge and at the mesoscale, commonly offset layers and lenses within the zone of fault rocks (Fig. 4). Granular gouge forms the next unit. In outcrop, granular gouge is 10–20 cm thick and commonly tabular. Compared to the other units, thickness changes of granular gouge are gradual. Granular gouge can be in direct contact with the detachment and hanging wall; however, more commonly, clay gouge occurs between granular gouge and the detachment. Clay gouge often displays evidence of mesoscopic ductility (Miller, 1996)—mixing, folding, flow, abrupt changes in unit thickness, and hanging wall injection. High shear strain, extreme comminution and syn-kinematic alteration to clay minerals, make it difficult to speculate on the origin of this unit. Unlike the other fault rock types observed, clay gouge could be allochthonous with respect to both the immediate hanging wall and footwall.

It is tempting to correlate the spatial progression described above (foliated breccia → granular gouge → clay gouge) with an evolutionary progression. Detailed chemical and mineralogical analyses of the Turtleback fault rocks and wall rocks are underway to determine the protoliths and fluid inputs necessary to account for the fault rock compositions. Because the fault rock thickness is modest (~1 m) despite a large amount of displacement (~2 km), the rate of incorporation of material into the zone of fault rocks must have been low relative to the shear rate. Therefore, a shear apparatus with parallel walls and constant gouge volume as is commonly used by experimentalists (Beeler and Tullis, 1995; Blanpied et al., 1995) is an appropriate analogy for both the fault gouge and breccia found along the detachment faults of Death Valley.

4.3. Thin section preparation and description

I collected about 100 samples of different fault rock types from more than 30 locations along the detachment fault system. In general, the rocks were coherent enough to sample and transport back to the laboratory. Then, using a hammer, chisel, file and dry saw, subsamples were created small enough to fit into 5 cm×3 cm plastic containers. In these plastic containers, the samples were immersed in LR White acrylic resin, placed in a vacuum for an hour, and soaked at $< 5^{\circ}C$ for 1–4 weeks. Then the epoxy and rock were cured at $60^{\circ}C$ for 24 hours. The epoxy-embedded samples were cut and thin sections made.

Eight fault gouge samples (five clay gouge and three granular gouge) were analyzed for survivor grain shape preferred orientation (Table 1). The ideal samples were easy to orient in the field, contained the distinctive survivor grain texture, and were removed from regions of the shear zone with planar and parallel side-walls. All thin sections of gouge show evidence of penetrative granular flow; a fabric defined by clay minerals, shape preferred orientations, cleavage, and parting surfaces. In most samples, survivor grains are visible from the scale of a hand sample (cm-sized survivors) down to the scale of SEM micrographs (10 μm-sized survivors).

Four foliated breccia samples were also analyzed for shape preferred orientation of fractured grains (Table 1). I found that if a fault breccia displays a planar texture in hand sample, it is defined by localized shear surfaces or fractures—not by a planar arrangement of material.

5. Shape preferred orientations in fault rocks

SPO data were collected by two independent methods: optical microscope and clast traces of electron microprobe images. The details of the methods developed for the collection and analysis of SPO data are covered in the Appendix A. Below, I argue that the results of the two methods provide an important confirmation of the significance of the SPO data.

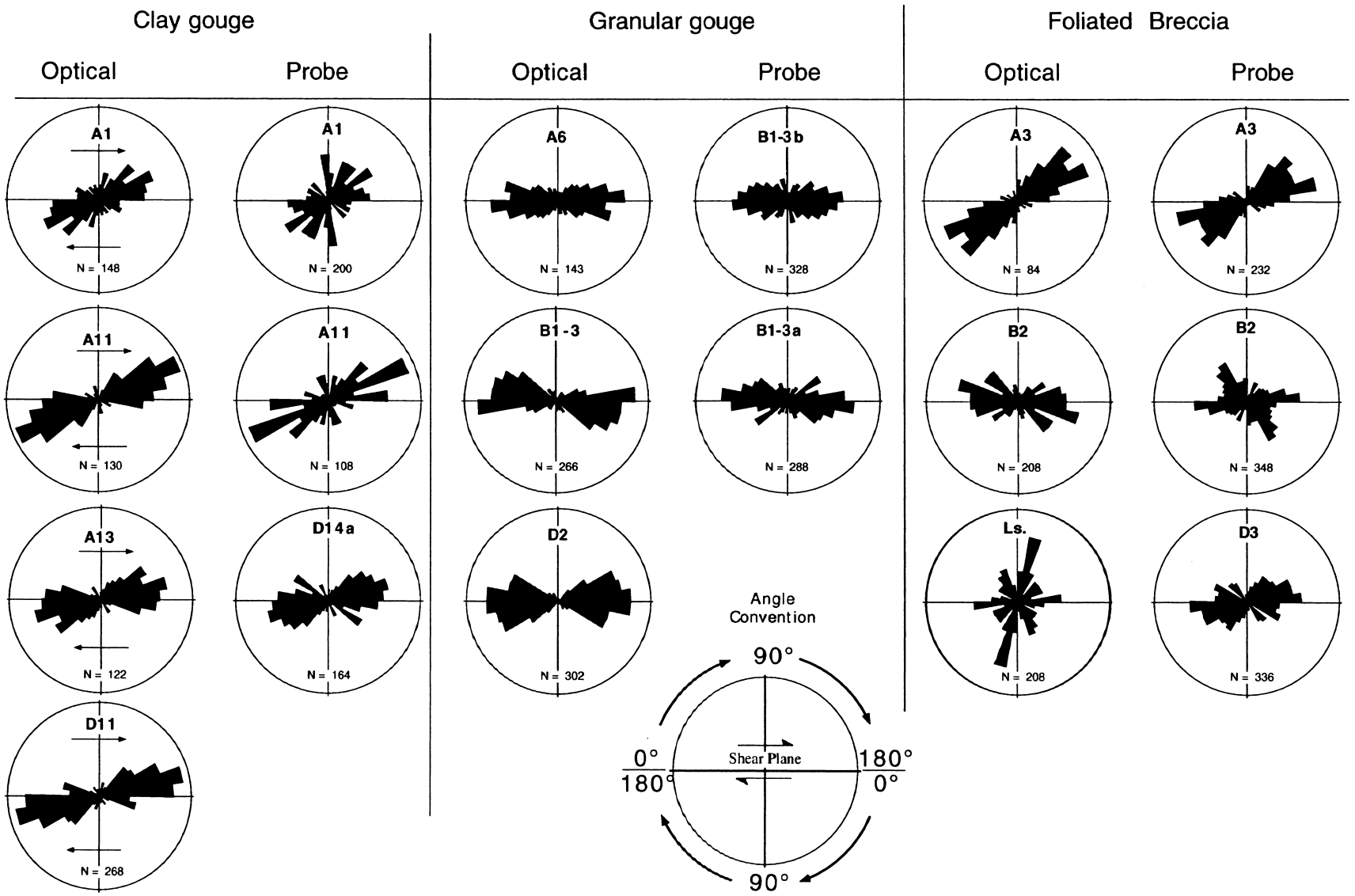

Fig. 5. Rose diagrams showing shape preferred orientations (SPO) of gouges and breccias. The circles represent 10% of data in all rose diagrams. Rose diagrams were created with R. W. Allmendinger's Stereonet 5.0.

Shape preferred orientations of survivor grains are surprisingly strong in fault gouge (Fig. 5). Clay gouges consistently have SPOs inclined to the shear plane by about 165°. In contrast, in granular gouge SPOs are roughly parallel to the shear plane. Some of the breccias have strong SPO (e.g. A3), but as a group the orientation and strength of SPOs in these are much less consistent than they are in the gouges. The breccia sample with the most evidence of cataclasis, a cataclastic limestone from the Keystone Thrust in southern Nevada provided to us by C. Sammis, has no significant SPO.

5.1. Different magnifications

Eqs. (A1) and (A2) allow a more sophisticated analysis of SPO than the rose diagrams of Fig. 5. For example, the variation of SPO with scale can be tested by calculating the vector mean and mean vector strength for the data sets collected at each magnification (Fig. 6, Table 2). For the optical data there was little variation of SPO (orientation and strength) with scale, especially for samples A1, A3, A11, and D2 (Fig. 6a). Even for samples with a large variation in mean vector strength (B1, B2, and A6), the mean vector orientation is nearly constant with scale. The greater variability of the vector mean and vector strength for the probe method was to be expected (Fig. 6b). Noise and heterogeneity is minimized for the optical data due to averaging across the thin section. Meanwhile, the probe data, collected at a single image at each magnification, would be unduly influenced by heterogeneity. In summary, it appears that SPO is not affected by the scale of data collection, at least in the range of scales analyzed here. Furthermore, the data collected at different scales and by different methods confirm that SPO data are reproducible.

5.2. Combined data sets

Fig. 7 consolidates the summary data from all magnifications for each sample. As qualitatively indicated by the rose diagrams (Fig. 5), the SPO strengths of clay gouges and granular gouges are similar, but the orientations are significantly different. In clay gouges, the mean SPOs are near 165° and in granular gouges, the SPOs are roughly parallel to the shear plane (180°). Fig. 7 also clearly shows that the SPOs in foliated breccias are variable.

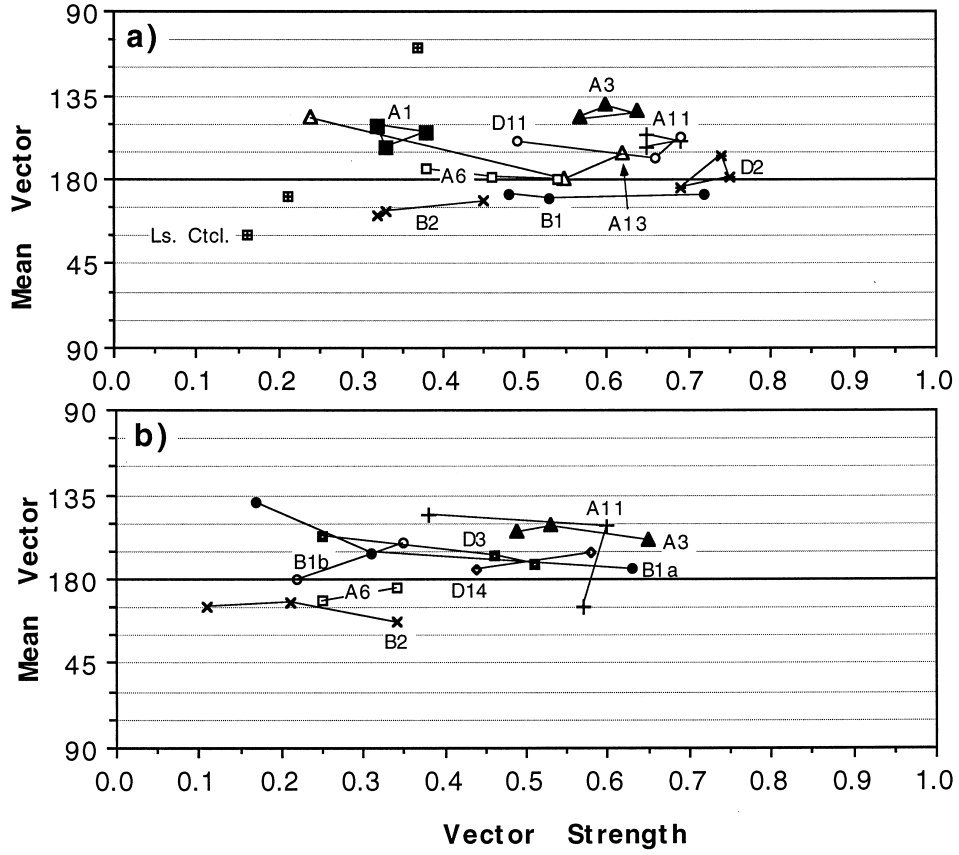

Fig. 6. Vector strength vs mean vector orientation for each sample at each magnification. Lines connect results obtained from different magnifications of the same sample. (a) Data collected by the optical microscope method. (b) Data collected by the microprobe image method.

Table 2
SPO results for 13 analyzed samples; including orientation and axial ratio data for populations combined from three magnifications

Sample	Optical data			Microprobe data		
	Mean vector	Vector strength	Average *R*	Mean vector	Vector strength	Average *R*
A1	156	0.34	1.96	140	0.26	1.79
A3	144	0.59	2.17	153	0.51	1.73
A6	178	0.46	1.90	19	0.27	1.66
A11	159	0.65	1.98	154	0.38	1.67
A13	164	0.56	2.05			
B1	9	0.59	1.89	2	0.36	1.60
B2	10	0.38	1.97	18	0.23	1.78
D2	176	0.71	1.78	75	0.12	1.74
D3				165	0.36	1.71
D11	163	0.59	1.81			
D14				170	0.50	1.80
CtLs	109	0.10	1.92			

5.3. Optical data vs probe data

Comparing Fig. 7(a) and (b) allows confirmation that the optical and probe methods give roughly similar results. The absolute vector strengths are consistently higher for the optical data. Again this was to be expected given that the optical method averages over the entire thin section.

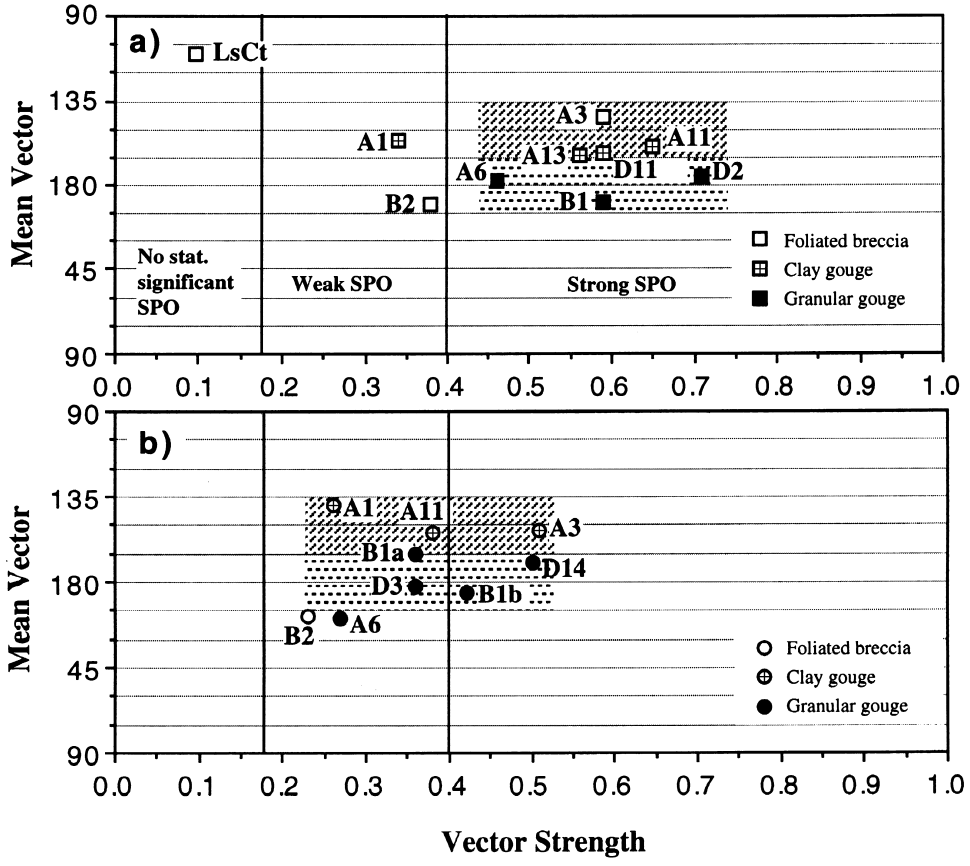

Fig. 7. Vector strength vs mean vector orientation for each sample. Because the results shown in Fig. 6 do not appear to depend upon magnification, the data collected at the various magnifications have been combined to one data point for each sample. (a) Data collected by the optical microscope method. (b) Data collected by the microprobe image method.

5.4. Axial ratios

As will be explained in the next section, the behavior of an elliptical particle in a shearing medium depends upon the particle's axial ratio. Therefore, it is also important to examine the axial ratios of the clasts used to determine the SPO. Fig. 8 shows axial ratio histograms for three typical samples and Table 2 gives the average axial ratios for all samples analyzed. The axial ratio populations are not significantly different for the 15 samples. For the optical data sets, the mean axial ratios range from 1.8 to 2.2. The population distribution for axial ratios less than 1.4 is a function of the data collection process, not the actual distribution of shapes; grain selection required that a clear orientation could be determined, which was not possible for the more equant grains ($R<1.4$). The axial ratio populations for the probe data sets more accurately reflect the actual distribution of shapes. Because the orientations of nearly equant grains were not considered robust, clasts with $R<1.4$ were removed from the probe data sets.

6. Numerical models for SPO

A final advantage of the vector mean and vector strength presentations (Figs. 6 and 7) is the ease with which the data can be compared to a numerical model. In this section a numerical model for the behavior of rigid clasts in a shearing medium is developed and synthetic results compared to the data of Figs. 6 and 7.

6.1. Theoretical background

Several recent theoretical and experimental studies have applied and modified the model originally proposed by Ghosh and Ramberg (1976) to explore general flow in shear zones and how kinematic parameters may be recorded in the fabric of natural faults (e.g. Means et al., 1980; Lister and Williams, 1983; Passchier, 1987; Hanmer and Passchier, 1991; Simpson and DePaor, 1993; Fossen et al., 1994; Masuda et al., 1995). The kinematic vorticity number W_k (e.g. Means et al., 1980; Passchier, 1987) is a traditional measure of vorticity for structural geologists studying plastically deformed fault rocks. For the numerical modeling below, I return to the ratio of pure shear rate to simple shear rate originally used by Ghosh and Ramberg (1976):

$$s = \frac{\dot{\varepsilon}}{\dot{\gamma}}. \tag{1}$$

Equation (4) of Ghosh and Ramberg (1976) gives the rotation rate of a rigid inclusion suspended in a viscous matrix as a function of s, the inclusion's orientation (φ) and axial ratio (R). Ghosh and Ramberg (1976) employ an alternative definition of the angle φ; rewriting in terms of the angle convention shown in Fig. 3, the rotation rate for a rigid inclusion becomes

$$\dot{\varphi} = \dot{\gamma}(A \sin^2 \varphi - B \sin 2\varphi + C \cos^2 \varphi), \tag{2}$$

where:

$$A = \frac{R^2}{R^2+1},\ B = \frac{s(R^2-1)}{R^2+1},\ \text{and}\ C = \frac{1}{R^2+1}.$$

Ghosh and Ramberg (1976) further show that a critical axial ratio divides the rotational behavior of clasts:

$$R_{crit} = \frac{1+\sqrt{1+4s^2}}{2s}. \tag{3}$$

For elongate clasts ($R \geq R_{crit}$), the rotation rate may be negative, positive, or zero depending of the orientation of the clast (see Simpson and DePaor, 1993 for more details). When $\dot{\varphi} = 0$, a clast is said to occupy a stable position. In a thickening shear zone ($s<0$), the orientation of the stable position is related to the ratio of pure shear and simple shear rates:

$$\varphi_1 = \tan^{-1}\left(-\frac{1}{2s}\right) + 90^\circ. \tag{4}$$

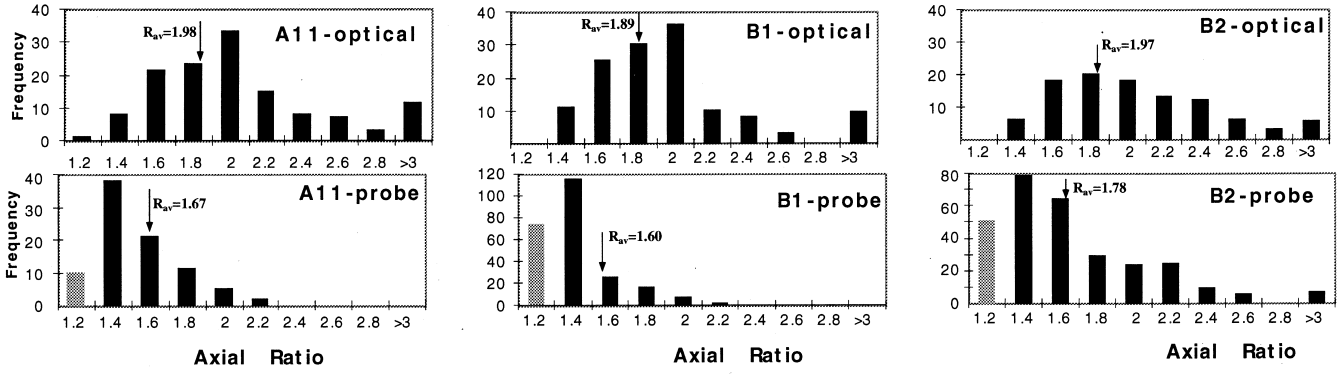

Fig. 8. Histograms of axial ratios for three samples shown in Fig. 2. Average axial ratios are also marked for each sample and method.

In a thinning shear zone ($s > 0$), the orientation of the stable position is always the shear plane:

$$\varphi_2 = 0^\circ = 180^\circ. \tag{5}$$

The orientations given by Eqs. (4) and (5), called eigenvectors of the flow (Bobyarchick, 1986), give the orientation of foliations defined by the most elongate clasts ($R \geq R_{crit}$). For flow regimes with $|s|<0.5$, the stable eigenvector is always between 135° and 180°, the P-foliation orientation (Fig. 9).

For more equant clasts ($R<R_{crit}$), rotation rates vary with orientation and the clasts always have a positive, non-zero rotation rate. The SPO developed by a population of rotating survivor grains will be related to the bisector of the stable and unstable eigenvectors (Fig. 9). The acute bisector of the eigenvectors is the orientation at which rotational velocity is at a minimum for rotating clasts and given by

$$\varphi_3 = \frac{1}{2}\tan^{-1}(2s) \tag{6}$$

(Ghosh and Ramberg, 1976). The obtuse bisector is the orientation at which clast rotation rate is a maximum. Thus at any time one would expect to find more

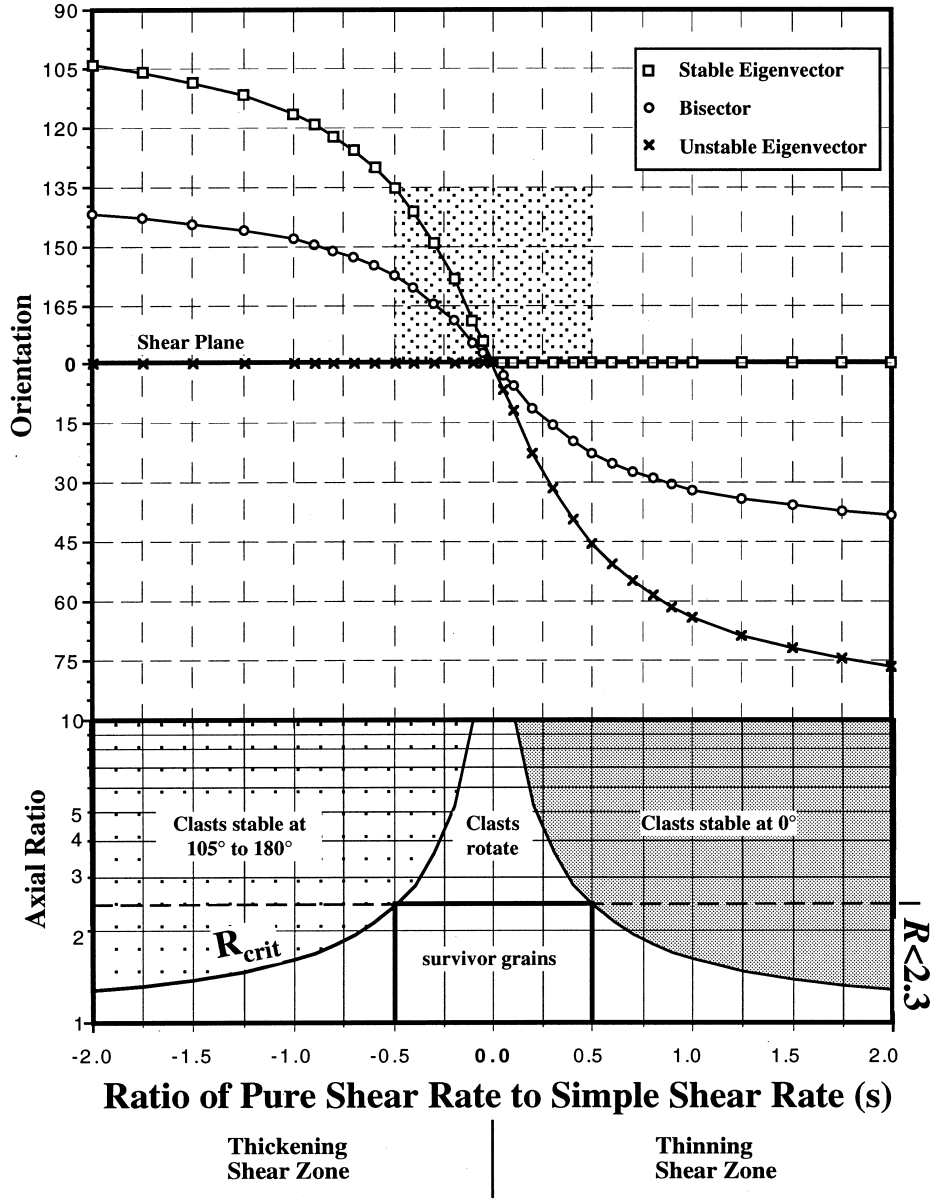

Fig. 9. Eigenvector orientations and critical axial ratio as a function of s, the ratio of pure shear rate to simple shear rate [Eqs. (3)–(5)]. The two boxes—the regions of most interest—are determined from the following observations and assumptions; (i) the vorticity in a brittle shear zone is mostly simple shear so $|s|<0.5$; (ii) the range of P-foliations is defined to be 135–180°; and (iii) most clasts in the natural data sets are relatively equant ($R<2.3$).

clasts with orientations near the acute bisector and away from the obtuse bisector. In the next section, this supposition is supported through numerical modeling.

In general, the value of s for a shear zone is not known a priori; therefore, it will also not be known whether the clasts in an orientation data set reached stable positions ($R \geq R_{crit}$) or continuously rotated ($R < R_{crit}$). Most of the survivor grains in the Death Valley data sets (Fig. 8) are relatively equant ($R < 2.3$); thus, as long as $|s| < 0.5$, the survivor grains would have continuously rotated during shear (Fig. 9). At $|s| = 0.5$, the pure shear rate is 50% of the simple shear rate. In other words, a shear zone with $s = -0.5$ would widen by 0.5 m for every 1 m of slip. While that may be locally possible, it seems safe to assume that $|s| < 0.5$ and $R_{crit} > 2.3$ for most regions of Death Valley brittle shear zones and that the survivor grains continuously rotated during shear.

6.2. Numerical modeling for more equant clasts

The shape preferred orientation displayed by survivor grains is a record of the penetrative strain experienced by the fault gouge. Numerical models based on Eq. (2) allow exploration of the formation, stability, and kinematic interpretation of the SPO observed in natural gouge. Using a Microsoft Excel spreadsheet and macro, the numerical model is applied as follows. First initial axial ratios and orientations are determined for >100 clasts for two synthetic data sets. The first synthetic clast population was modeled on the real data collected for sample B1: 134 clasts with an axial ratio distribution as measured by the optical method on sample B1 (Fig. 8). Unlike B1, random initial orientations between 0° and 180° were chosen for each clast. In the second synthetic population, the behavior of passive markers was explored by setting $R = \infty$ for 100 clasts. Once setup was complete, the angular rotation of each clast due to a small amount of shear ($\gamma = 0.02$) was calculated from Eq. (2) and then used to find a new orientation. This step was repeated until a high shear strain ($\gamma = 10$) accumulated. To track the behavior of the synthetic clast populations, the vector mean [Eq. (A1)] and the mean vector strength [Eq. (A2)] were calculated after each shear increment of 0.25 (Fig. 10). Masuda et al. (1995) also used Eq. (2) to model the behavior of populations of rigid clasts. They presented the synthetic data as R vs φ diagrams, which prove to be much less useful than summarizing shape preferred populations with the mean vector and vector strength as is shown below.

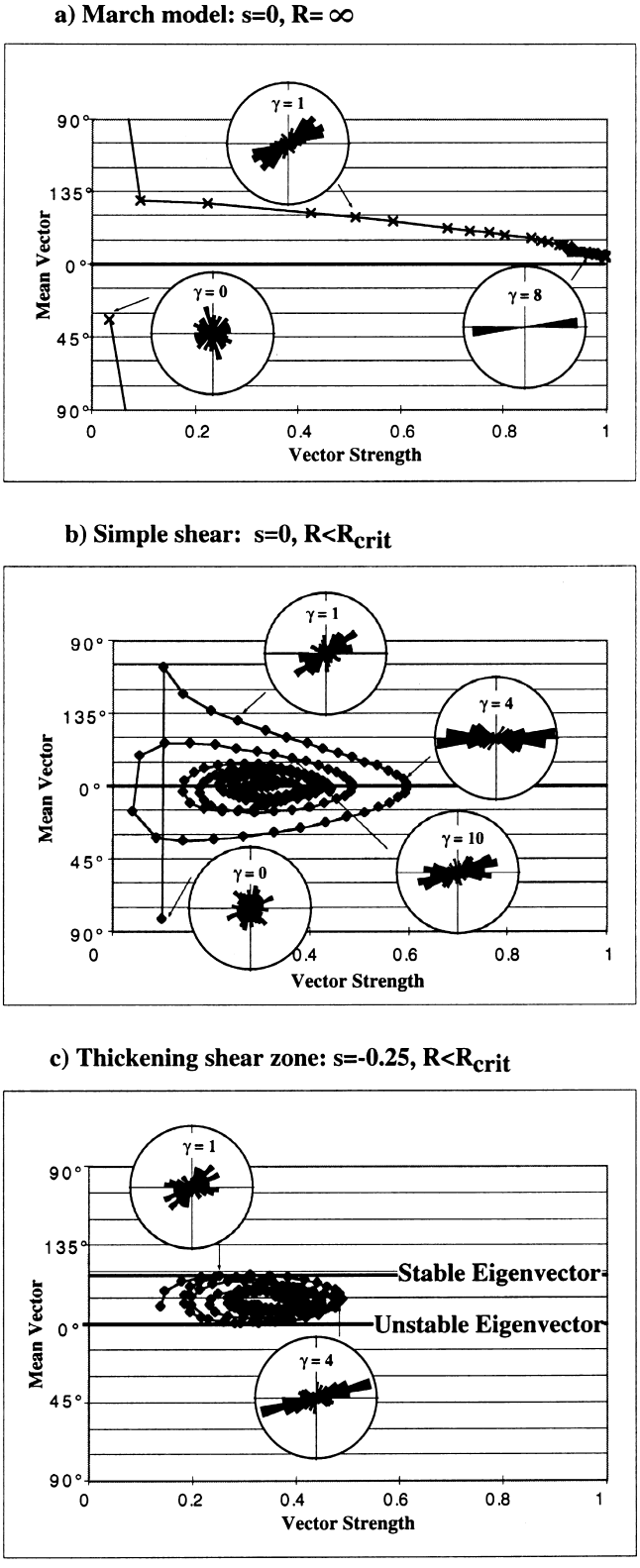

Fig. 10. Graphs of vector strength vs mean vector orientation for synthetic data; points represent shear strain increments of 0.25. Rose diagrams give qualitative view of SPO at various shear strains.

6.3. Synthetic results

For the simulation of the simple shear March model, the mean orientation formed near 135° at low ($\gamma = 0.25$) shear strain, then increased toward 180° with increasing shear strain as all clasts within the population reached their stable positions of 180° (Fig. 10a). The vector strength also increased toward 1.0 with shear strain. In contrast, elongate rigid clasts in simple shear (simple shear Jeffery model) developed an SPO, yet the mean orientation and vector strength never reached stable values (Fig. 10b). Rather, the values orbited as all clasts continued to rotate. Again, the mean orientation of the rotating clasts varied about the shear plane ($\varphi = 0° = 180°$). In summary, after high simple shear strain, populations of both passive and non-passive clasts define an SPO which, on average, is parallel to the shear plane.

In order to develop an SPO inclined to the shear plane, the pure shear component of the deformation must be non-zero ($s \neq 0$). In the example shown in Fig. 10(c), the mean orientation of a population of rigid clasts attains an inclined but pulsing orientation with an orientation defined by the bisector of the two eigenvectors. In summary, the synthetic models show that an inclined SPO of survivor clasts ($R<R_{crit}$) can be formed in a thickening ($s<0$) shear zone.

7. Uncertainties

Before proceeding with the implications of the SPO data and modeling, a brief discussion of uncertainties is necessary.

7.1. Field and data collection uncertainties

It is difficult to maintain orientation of the sample during field sampling, laboratory sub-sampling, epoxying, and thin sectioning. Up to 15° of orientation error is possible if no internal marker is present which can be followed from field sample to thin section. Fortunately, this type of error was minimized due to preservation of the fault plane within the thin section in most samples (A11, A13, A3, D11, D14, B2). In other cases, fault plane parallel flow-banding was obvious in thin section and outcrop (B1, D2).

Morgan and Cladouhos (1995), Miller (1996), and Cowan et al. (1997) have documented rapid changes in fault rock unit thickness and in many cases the fabric or flow-banding is affected by local heterogeneity of this sort. The samples analyzed for SPO were chosen from regions of shear zones with planar, parallel-sided walls; however, the limitations of incomplete two-dimensional outcrops make it difficult to rule out rapid changes in the shear zone thickness near any sampling locality. Even in the case of perfect outcrop, the actual width of the actively deforming zone may not have corresponded to the width of the fault rock unit. The effect of local heterogeneity cannot be downplayed; however, it is encouraging that the SPO data seems to be internally consistent with fault rock type. The SPO data may be evidence in itself that local heterogeneity is overwhelmed by global consistency.

Survivor grain shape preferred orientation has not previously been reported from fault gouge SPO. Three observations add strength to the conclusion that the SPO is real—not an artifact of the data collection methodology. First, despite important differences between the data collection methodologies (see Appendix A), there is rough agreement (compare Fig. 6a and b and Fig. 7a and b) between the SPO data derived from microprobe images interpreted by image analysis software and the SPO data collected on an optical microscope. Second, although it is usually not possible to discern an SPO in a hand sample, we have often observed SPO in pebble- and cobble-sized clasts within shear zones at the outcrop scale. Third, P-foliations, inclined to the shear plane, have been reported by many (Logan et al., 1979; Rutter et al., 1986; Chester and Logan, 1987). SPO is one component of the P-foliation observed by others.

7.2. Model uncertainties

Ghosh and Ramberg (1976) explicitly state that their model applies to the behavior of rigid clasts in a viscous matrix. Whether a viscous rheology is appropriate for a fine-grained clay matrix at the temperature, pressure, and fluid conditions at which the deformation occurred is an open question. An equally important question is whether the rheology of the matrix matters for equations which are fundamentally kinematic. Another potential problem with the Ghosh and Ramberg (1976) model is that the interface between the matrix and the rigid clasts is assumed to be slip free. Again, the importance of this assumption and the degree to which it is violated when applied to fault gouge are difficult to ascertain. Despite these possible problems, the Ghosh and Ramberg (1976) model offers the best framework under which to understand SPO in fault gouge. It is familiar to many structural geologists, is at heart kinematic, and roughly appears to fit the data.

8. Discussion and conclusion

This contribution started with a description of fault rocks, proceeded to the collection of SPO data sets, and concluded with the application of well known theory to the newly collected data sets. Each phase of this

work has important implications for the kinematics and rheology of the materials found in brittle shear zones; I start at the most fundamental and perhaps most profound.

8.1. Survivor grain texture

Fault gouges display a texture characterized by survivor grains in a matrix. This texture has been recognized before (Engelder, 1974); however, its significance and usefulness have not been appreciated. Several features of the survivor grain texture allow dismissal of uncertainties commonly cited when analyzing the kinematics of naturally and experimentally deformed rock samples (i.e. Tullis, 1976; Oertel, 1985). The survivor grains show no evidence of crystal–plastic deformation, dissolution, or mineral growth. Survivor grains are subrounded and isolated from other grains of similar size suggesting that grain fracture and grain-to-grain interaction were minimal in the latter stages of deformation. The matrix in which the survivor grains are embedded, composed of either clay or comminuted parent material, is commonly foliated or banded, indicating penetrative flow. All of the above observations suggest that survivor grains can be treated as rigid clasts in a viscous flow as modeled by Ghosh and Ramberg (1976). In fact, survivor grains may offer one of the best applications yet of the theoretical model. In addition, because the texture precludes grain fracture, it suggests that the flow was not cataclastic, but rather shearing particulate flow.

8.2. Existence and strength of shape preferred orientation

The long axes of elongate ($R > 1.4$) survivor grains show profound preferred orientations in most samples and at most scales. This result was unexpected; the eye does not discern a shape preferred orientation in Fig. 2(c) or (e). Data collection by either optical microscope or computer analysis of microprobe images eliminates the noise introduced by more equant grains and statistically significant SPOs become apparent (Figs. 5–7). In addition, gouge samples of similar type have consistent orientations of SPO. In clay gouges, the mean vectors of the SPOs determined by the optical method are inclined to the shear plane by ~165°. In granular gouge, the mean vectors of the SPOs are sub-parallel to the shear plane (inclinations from 175° to 10°). The existence and consistency of SPO is further evidence that deformation was penetrative, homogeneous, and of a type that can be simulated by a relatively simple model. Furthermore, as the development of a SPO of rigid clasts is not instantaneous, the parameters of the deformation must have been steady for a relatively large increment of shear ($\gamma > 3$).

8.3. Numerical modeling

Finally, the adoption of two models which predict the behavior of clasts in a shearing flow allows further

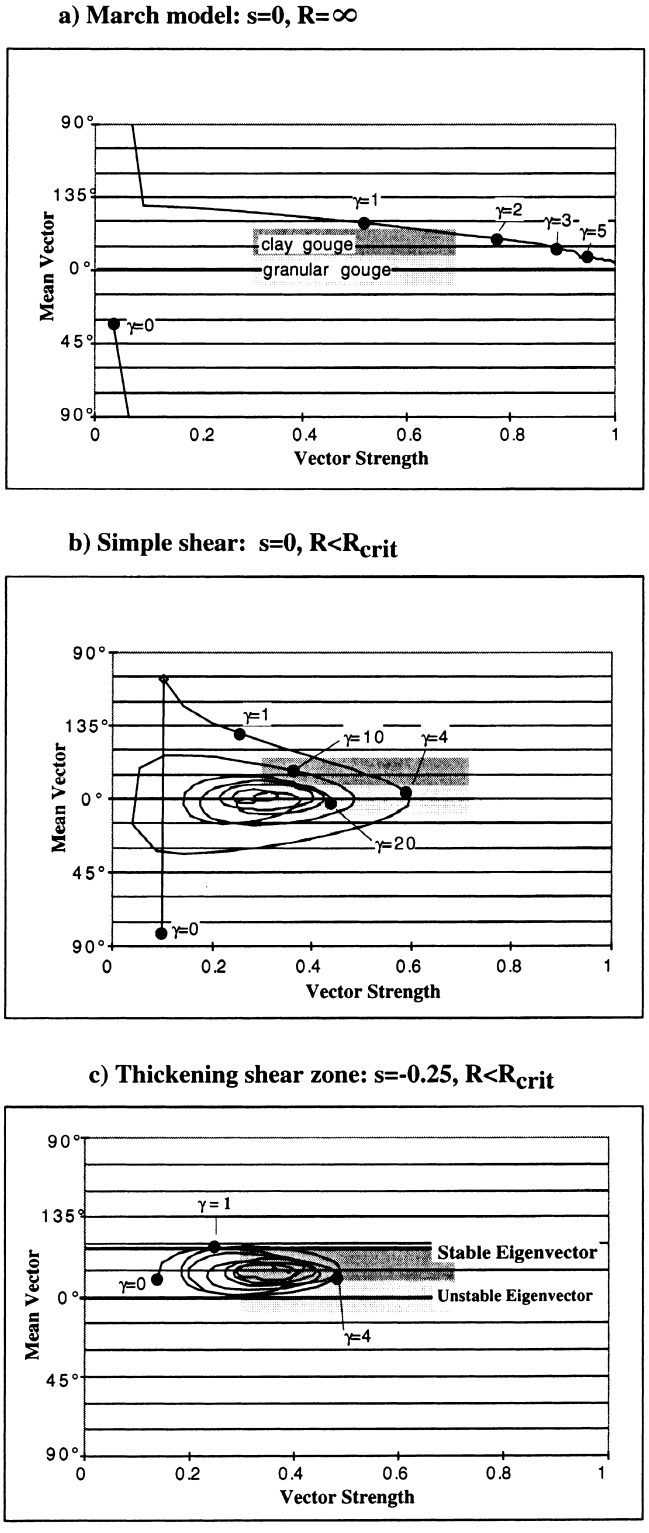

Fig. 11. Superposition of model results (from Fig. 10a, b, and c) and natural SPO data (from Fig. 7a).

interpretation of the SPO results. A direct comparison of natural SPO data and synthetic results (Fig. 11) highlights the primary implication of the modeling portion of this paper. If survivor grains behaved as March markers, then the shear strain must have been low ($\gamma<3$) in clay gouges, but could have been unlimited in granular gouges. If the survivor grains behaved as rigid clasts in general shear, then foliated clay gouges record thickening shear zones ($s\approx -0.25$) while flow-banded granular gouges record simple shear ($s\approx 0$). Intuitively, shear zone thickening cannot be a steady state solution for a brittle shear zone. In the following paper (Cladouhos, 1999), a steady state kinematic model is developed to explain the apparent shear zone thickening evidenced by the SPO data and inclined P-foliation in general.

Acknowledgements

This work was performed under NSF grant #EAR-9417759 to Darrel S. Cowan at the University of Washington. I thank D. S. Cowan and J. K. Morgan for their help throughout the project. I also thank D. McDougal for thin section preparation of extremely challenging rocks. Nick Beeler and Haakon Fossen provided valuable reviews of the manuscript.

Appendix A

A.1. Shape orientation data collection

Shape orientation data were collected by two independent methods: optical microscope and clast traces of electron microprobe images. Data collection by optical microscope was done in a traditional manner (e.g. Shelley, 1995). Thin sections were systematically traversed by placing in a counting stage with the down-dip direction pointing south. Roughly elliptical, isolated (not touching another grain of a similar size) clasts were selected and the length of the long and short axes and the orientation of the long axis with respect to the shear plane (see convention in Fig. 3) were measured. Each thin section was traversed at three different magnifications (31.25×, 125×, and 312.5×) until around 50 grains (150 total) were measured. Care was taken not to measure the same clast twice.

The second method employed digitized black and white images of clasts which were made as part of a study of the particle size distributions of gouge. Three image scales were used. For the lowest magnification, each thin section was placed in the negative slot of a black and white photo enlarger, and a black and white print was made. The print was then digitized on a flatbed scanner. This digital image corresponded to a magnification of 7×. For higher magnifications, electron microprobe images taken at 48× and 200× were digitally captured at a resolution of 300 dpi using Gatan's Digital Micrograph. I attempted to use image processing software to classify clasts and matrix; however, this proved unfeasible as the gray-scale contrast between clasts and matrix or between clast boundaries and matrix was too subtle for automated classification. Instead, the images were imported to a graphics program where the outlines of clasts were traced (polygonized). The clast maps were converted to binary bitmap images and then, using the public domain software NIH Image, the lengths and orientations of the major and minor axis were determined for each clast. Because the clast maps were created for particle size distribution analysis, the data included many clasts with low axial ratios. For use as SPO data, all clasts with $R<1.4$ were eliminated as the orientation of nearly equant clasts is not robust.

Data collection by two independent methods provides an important confirmation of the significance of the SPO data. The most basic difference between the methods is that the optical method relies upon the microscope operator to select clasts which are elliptical and isolated. Because the entire thin section is traversed, but not all clasts are selected, the optical method includes a step of subjective interpretation that could potentially introduce a bias. In contrast, the probe technique relies on a computer fit of an ellipse to sometimes irregularly shaped clasts to determine an SPO for all clasts in one image regardless of clast shapes or isolation. The data show that despite these differences, the two methods give quite similar results. The optical method produces much cleaner SPO data sets, but both methods give similar orientations of SPO.

A.2. Data analysis

Rose diagrams provide a qualitative and visual assessment of both the orientation and intensity of the shape preferred orientation. A quantitative derivation of these parameters provides further insight. To find the mean orientation of N clasts with orientations θ_i the semicircular vector mean ($\hat{\mathbf{V}}$) is calculated (Agterberg, 1974),

$$\hat{\mathbf{V}} = \frac{1}{2}\tan^{-1}\left(\frac{\sum \sin 2\theta_i}{\sum \cos 2\theta_i}\right) \tag{A1}$$

where i is summed from 1 to N. The mean vector strength ($\bar{a}$) measures the scatter of the unit vectors summed in Eq. (A1):

$$\bar{a} = \frac{1}{N}\left\{\left(\sum \sin 2\theta_i\right)^2 + \left(\sum \cos 2\theta_i\right)^2\right\}^{1/2}. \quad \text{(A2)}$$

If all unit vectors are parallel, then $\bar{a} = 1$. If the unit vectors are uniformly distributed about a semicircle, then $\bar{a} = 0$. In general, a random arrangement of unit vectors will have $\bar{a} > 0$, so a value of $\bar{a}$ must be defined to separate a statistically significant preferred orientation of vectors from a statistically random orientation. To determine the maximum likely vector strength generated by random data, a numerical model was created. The vector mean and vector strength of 100 vectors with random orientations was calculated for 100 different data sets. In 95% of the trials $\bar{a} < 0.17$, so this value is used as the lowest value of a statistically significant SPO.

References

Agterberg, F.P., 1974. Geomathematics. Elsevier Science, Amsterdam.

An, L.-J., Sammis, C.G., 1994. Particle size distribution of cataclastic fault materials from southern California: A 3-D study. Pure and Applied Geophysics 143, 203–227.

Beeler, N.M., Tullis, T.E., 1995. Implications of Coulomb plasticity for the velocity dependence of experimental faults. Pure and Applied Geophysics 144, 251–276.

Blanpied, M.L., Lockner, D.A., Byerlee, J.D., 1995. Frictional slip of granite at hydrothermal conditions. Journal of Geophysical Research 100, 13045–13064.

Bobyarchick, A.R., 1986. The eigenvalues of steady flow in Mohr space. Tectonophysics 122, 35–51.

Chester, F.M., Logan, J.M., 1987. Composite planar fabric of gouge from the Punchbowl Fault, California. Journal of Structural Geology 9, 621–634.

Chester, F.M., Friedman, M., Logan, J.M., 1985. Foliated cataclasites. Tectonophysics 111, 139–146.

Cladouhos, T.T., 1999. A kinematic model for deformation within brittle shear zones. Journal of Structural Geology 21, 437–448.

Cowan, D.S., Brandon, M.T., 1994. A symmetry-based method for kinematic analysis of large-slip brittle fault zones. American Journal of Science 294, 257–306.

Drewes, H., 1963. Geology of the Funeral Peak Quadrangle, California, on the eastern flank of Death Valley. U.S. Geological Survey Professional Paper 413, 78 pp.

Engelder, J.T., 1974. Cataclasis and the generation of fault gouge. Geological Society of America Bulletin 85, 1515–1522.

Erickson, S.G., 1990. Mechanics of deformation and thrust fault zones. Unpublished PhD dissertation, Texas A&M University, College Station, Texas, USA.

Erickson, S.G., Wiltschko, D.V., 1991. Spatially heterogeneous strength in a thrust fault zones. Journal of Geophysical Research 96, 8427–8440.

Fossen, H., Tikoff, B., Teyssier, C., 1994. Strain modeling of transpressional and transtensional deformation. Norsk Geologisk Tidsskrift 74, 134–145.

Ghosh, S.K., Ramberg, H., 1976. Reorientation of inclusions by combination of pure shear and simple shear. Tectonophysics 34, 1–70.

Gretener, P.E., 1977. On the character of thrust faults with particular reference to the basal tongues. Bulletin of Canadian Petroleum Geology 25, 110–122.

Hanmer, S., Passchier, C., 1991. Shear-sense indicators: a review. Geological Survey of Canada, Paper 90-17, 72 pp.

Holm, D.K., Wernicke, B., 1990. Black Mountains crustal section, Death Valley extended terrain, California. Geology 18, 520–523.

Holm, D.K., Snow, J.K., Lux, D.R., 1992. Thermal and barometric constraints on the intrusive and unroofing history of the Black Mountains: Implications for timing, initial dip, and kinematics of detachment faulting in the Death Valley region, California. Tectonics 11, 507–522.

Jeffery, G.B., 1922. The motion of ellipsoidal particles immersed in a viscous liquid. Proceedings of the Royal Society of London, Series A 102, 161–179.

Lister, G.S., Williams, P.F., 1983. The partitioning of deformation in flowing rock masses. Tectonophysics 92, 1–33.

Logan, J.M., Friedman, M., Higgs, N., Dengo, C., Shimamoto, T., 1979. Experimental studies of simulated gouge and their application to studies of natural fault zones. In: Proceedings of Conference VIII on Analysis of Actual Fault Zones in Bedrock: U.S. Geological Survey Open-File Report 79-1239.

March, A., 1932. Mathematische theorie der regelung nach der korngestalt bei affiner deformation. Zeitschrift für Kristallographie 81, 285–297.

Masuda, T., Michibayashi, K., Ohta, H., 1995. Shape preferred orientation of rigid partical in a viscous matrix: reevaluation to determine kinematic parameters of ductile deformation. Journal of Structural Geology 17, 115–129.

Means, W.D., Hobbs, B.E., Lister, G.S., Williams, P.F., 1980. Vorticity and non-coaxiality in progressive deformation. Journal of Structural Geology 2, 371–378.

Miller, M.G., 1991a. High-angle origin of the currently low-angle Badwater Turtleback fault, Death Valley, California. Geology 19, 372–375.

Miller, M.G., 1991b. Brittle faulting induced by ductile deformation of rheologically stratified rock sequence, Badwater Turtleback, Death Valley, California. Geological Society of America Bulletin 104, 1376–1385.

Miller, M.G., 1992. Structural and kinematic evolution of the Badwater Turtleback, Death Valley, California. Unpublished PhD dissertation, University of Washington, Seattle, Washington.

Miller, M.G., 1996. Ductility in fault gouge from a normal fault system, Death Valley, California—A mechanism for fault-zone strengthening and relevance to paleoseismicity. Geology 24, 603–606.

Morgan, J.K., Cladouhos, T.T., 1995. Microstructures and fabrics of granular gouges from the Copper Canyon Detachment Fault, Death Valley. EOS 75 (46), F576.

Oertel, G., 1985. Reorientation due to grain shape. In: Wenk, H.-R. (Ed.), Preferred Orientation in Deformed Metals and Rocks: An Introduction to Texture Analysis. Academic Press, London, pp. 259–266.

Passchier, C.W., 1987. Stable positions of rigid objects in non-coaxial flow—a study in vorticity analysis. Journal of Structural Geology 9, 679–690.

Passchier, C.W., Simpson, C., 1986. Porphyroclast systems as kinematic indicators. Journal of Structural Geology 8, 831–843.

Passchier, C.W., Sokoutis, D., 1993. Experimental modelling of mantled porphyroclasts. Journal of Structural Geology 15, 895–909.

Pavlis, T.L., Serpa, L.F., Keener, C., 1993. Role of seismogenic processes in fault-rock development: An example from Death Valley, California. Geology 21, 267–270.

Ramsay, J.G., Huber, M.I., 1983. The Techniques of Modern Structural Geology. Academic Press, London.

Rutter, E.H., Maddock, R.H., Hall, S.H., White, S.H., 1986. Comparative microstructures of natural and experimentally pro-

duced clay-bearing fault gouges. Pure and Applied Geophysics 124, 3–30.

Scholz, C., 1990. The Mechanics of Earthquakes and Faulting. Cambridge University Press, Cambridge.

Scott, D.R., Marone, C.J., Sammis, C.G., 1994. The apparent friction of granular fault gouge in sheared layers. Journal of Geophysical Research 99, 7231–7246.

Shelley, D., 1993. Igneous and Metamorphic Rocks Under the Microscope. Chapman & Hall, London.

Shelley, D., 1995. Asymmetric shape preferred orientations as shear-sense indicators. Journal of Structural Geology 17, 509–517.

Sibson, R.H., 1977. Fault rocks and fault mechanics. Journal of the Geological Society of London 133, 191–213.

Simpson, C., DePaor, D.G., 1993. Strain and kinematic analysis in general shear zones. Journal of Structural Geology 15, 1–20.

Sorby, H.C., 1853. On the origin of slaty cleavage. Edinburgh New Philosophical Journal 55, 137–148.

Tullis, T.E. 1976. Experiments on the origin of slaty cleavage and schistosity. Geological Society of America Bulletin 87, 745–753.

Twiss, R.J., Moores, E.M., 1992. Structural Geology. W.H. Freeman, New York.

Wernicke, B., Axen, G.J., Snow, J.K., 1988. Basin and Range extensional tectonics at the latitude of Las Vegas, Nevada. Geological Society of America Bulletin 100, 1738–1757.

Wernicke, B.P., Hodges, K.V., Walker, J.D., 1986. Geological setting of the Tucki Mountain area, Death Valley National Monument, California. In: Wernicke, B.P., Hodges, K.V., Walker, J.D. (Eds.), Guidebook and Volume, Field Trips 2 and 14, 82nd Annual Meeting of Cordilleran Section, Geological Society of America, pp. 67–80.

Wise, D.U., Dunn, D.E., Engelder, J.T., Geiser, P.A., Hatcher, R.D., Kish, S.A., Odom, A.L., Schamel, S., 1984. Fault-related rocks: Suggestion for terminology. Geology 12, 391–394.

Wright, L.A., Troxel, B.W., 1984. Geology of the north 1/2 Confidence Hills 15′ Quadrangle, Inyo County, California, scale 1:24,000. California Division of Mines and Geology, Map Sheet 34, 31 pp.